Available online at www.sciencedirect.com
SCIENCE DIRECT®
Polymer 44 (2003) 5323–5339
polymer
www.elsevier.com/locate/polymer

Polycarbonate nanocomposites. Part 1. Effect of organoclay structure on morphology and properties

P.J. Yoon[a], D.L. Hunter[b], D.R. Paul[a,*]

[a]*Department of Chemical Engineering and Texas Materials Institute, The University of Texas at Austin, Austin, TX 78712-1065, USA*
[b]*Southern Clay Products, 1212 Church St., Gonzales, TX 78629, USA*

Received 11 March 2003; received in revised form 6 June 2003; accepted 9 June 2003

Abstract

Polycarbonate nanocomposites were prepared by melt processing from a series of organoclays based on sodium montmorillonite exchanged with various amine surfactants. To explore the effects of matrix molecular weight on dispersion, an organoclay was melt-mixed with a medium molecular weight polycarbonate (MMW-PC) and a high molecular weight polycarbonate (HMW-PC) using a twin screw extruder. The effects of surfactant chemical structure on the morphology and physical properties were explored for nanocomposites formed from HMW-PC. Wide angle X-ray scattering, transmission electron microscopy, and stress–strain behavior were employed to investigate the nanocomposite morphology and physical properties. The modulus enhancement is greater for nanocomposites formed from HMW-PC than MMW-PC. This trend is attributed to the higher shear stress generated during melt processing. A surfactant having both polyoxyethylene and octadecyl tails shows the most significant improvement in modulus with some of the clay platelets fully exfoliated. However, the nanocomposites formed from a range of other organoclays contained both intercalated tactoids and collapsed clay particles with few, if any, exfoliated platelets.

Keywords: Polycarbonate; Nanocomposites; Melt processing

1. Introduction

Polymer layered silicate nanocomposites have been the subject of many recent papers; this interest is mainly driven by the promise of strongly enhanced physical properties from well-exfoliated clay platelets in matrices such as nylon 6, polyimides, and epoxies. In principle, small amounts of these nanofillers, in the range of 3–5% by weight, can provide comparable properties as 20–30% of micro-sized fillers do in conventional composites. However, to achieve such properties in nanocomposites requires high levels of dispersion of the organoclay which is possible when there is good affinity of the polymer for the clay. When the polymer-organoclay interaction is not favorable enough to give well-exfoliated aluminosilicate platelets, then intercalated or partially exfoliated structures are usually obtained [1–10].

Polycarbonate has been modified and tailored in many different ways, particularly by blending with other polymers for use in demanding applications particularly when its outstanding impact strength is important [11]. There is very little information available in the literature relating to polycarbonate nanocomposites. In principle, addition of well-dispersed nanofillers to polycarbonate could preserve the optical clarity of this amorphous polymer. The promise of transparency plus improved stiffness and scratch resistance make a compelling case for exploring polycarbonate nanocomposites, particularly if toughness could also be preserved. Recently, Huang et al. reported on polycarbonate-layered silicate nanocomposites prepared by two different methods [12]. A partially exfoliated structure was obtained via ring opening polymerization from cyclic oligomers but intercalated layers were obtained via melt mixing in a Brabender mixer using linear polycarbonate. Severe et al. studied the thermal stability of polycarbonate nanocomposites formed in a twin screw extruder using phosphonium exchanged montmorillonite and synthetic clays [13]. They found that the phosphonium exchanged montmorillonite provided better thermal stability than synthetic clays. However, the effects of the chemical

* Corresponding author. Tel.: +1-512-471-5392; fax: +1-512-471-0542.
E-mail address: drp@che.utexas.edu (D.R. Paul).

0032-3861/03/$ - see front matter © 2003 Published by Elsevier Ltd.
doi:10.1016/S0032-3861(03)00528-7

structure of the organoclay, the molecular weight of the polycarbonate matrix, processing versus thermal degradation, color issues, etc. are poorly understood at this point.

The objective of this study is to explore the effect of matrix molecular weight and organoclay structure on the morphology and properties of polycarbonate nanocomposites. The main focus of this paper is to determine the extent that organoclays can be dispersed in a polycarbonate matrix by high shear melt processing. Various techniques including wide angle X-ray scattering (WAXS) and transmission electron microscopy (TEM) are used to examine the nanocomposite morphology and its effect on physical properties like stress–strain behavior and impact strength. A subsequent paper will discuss chemical issues, including degradation and color formation, and the influence of various processing variables during melt processing. The level of exfoliation of the aluminosilicate platelets reported here for polycarbonate is far less than that reported recently for nylon 6 [14,15] and the problems of degradation and color formation are more severe. Therefore, it is imperative to study the origin of these obstacles to formation of excellent nanocomposites based on polycarbonate and their relationship to the variables of melt processing.

2. Experimental

2.1. Polycarbonate materials

Two commercial polycarbonates, supplied by Mitsubishi Engineering Plastics Corp., that represent medium and high molecular weight grades, referred to here as MMW and HMW, respectively, were chosen for this study [16]. The physical form and molecular weight of these materials are described in Table 1.

2.2. Organoclays

The organoclays, supplied by Southern Clay Products, Inc., were formed by cation exchange between sodium montmorillonite, Na^{+}MMT, (CEC = 92 meq/100 g clay) and the various amine compounds described in Fig. 1. The nomenclature system, defined in a prior paper [15], uses various abbreviations to represent the substituents on the amine nitrogen, e.g. M for methyl, H for hydrogen, (HE) for 2-hydroxy-ethyl, B for benzyl, (EO) for ethylene oxide, and (PO) for propylene oxide substituents while T, (HT), and (C_{18}) represent long alkyl chains from natural tallow oil, hydrogenated tallow, and octadecyl hydrocarbons, respectively. Further details about the degree of saturation and exchange reaction between sodium montmorillonite and the onium compounds can be found in the previous and subsequent papers [15,17].

The organoclays were selected to explore the effects of the amine surfactant structure on the dispersion of clay particles in polycarbonate matrices. This series compares one at a time the effects of the number of alkyl tails, hydroxy-ethyl versus methyl, hydroxy-ethyl versus polyoxyethylene, quaternary versus tertiary ammoniums, degree of saturation, and size of substituents. The exchange amount expressed as the milliequivalent ratio (MER) and X-ray based d-spacings for these organoclays are summarized in Table 2.

2.3. Melt processing

Melt compounded composites were prepared using a Haake, co-rotating, intermeshing twin screw extruder (diameter = 30 mm, $L/D = 10$) using a barrel temperature of 260 °C, a screw speed of 280 rpm, and a feed rate of 980 g/h. Polycarbonate materials were dried in a vacuum oven at 80 °C for a minimum of 16 h prior to the compounding while the organoclay was used as received. Typical moisture content in the organoclays varies from 1 to 2 wt% and as much as 6 wt% in sodium montmorillonite corresponding to about 0.03 wt% in the compounded materials. Note that maximum allowable moisture content for molding of polycarbonate is 0.03 wt% [18] and a preferred level for extrusion is about 0.02 wt% [19].

Tensile (ASTM D638) and Izod specimens (ASTM D256) were formed using an Arburg Allrounder 305-210-700 injection molding machine operating at a barrel temperature of 280 °C, mold temperature of 80 °C, injection pressure of 75 bar, and a holding pressure of 35 bar. After molding, the specimens were immediately sealed in a polyethylene bag and placed in a vacuum desiccator for a minimum of 24 h prior to mechanical testing (Table 3).

2.4. Mechanical testing

Tensile tests were performed at room temperature according to ASTM D696 using an Instron model 1137

Table 1
Polycarbonates used in this study

Designation used here	Commercial designation	Form	Melt index	Specifications[a]	Supplier
MMW-PC	Iupilon S3000	Pellet	16.5	$M_n = 8500$	Mitsubishi Engineering Plastics Corp.
	Iupilon S2000F	Flake	16.5	$M_w = 23,700$	
HMW-PC	Iupilon E2000	Pellet	5.0	$M_n = 10,800$	Mitsubishi Engineering Plastics Corp.
	Iupilon E2000F	Flake	5.0	$M_n = 32,000$	

[a] Determined via GPC [16].

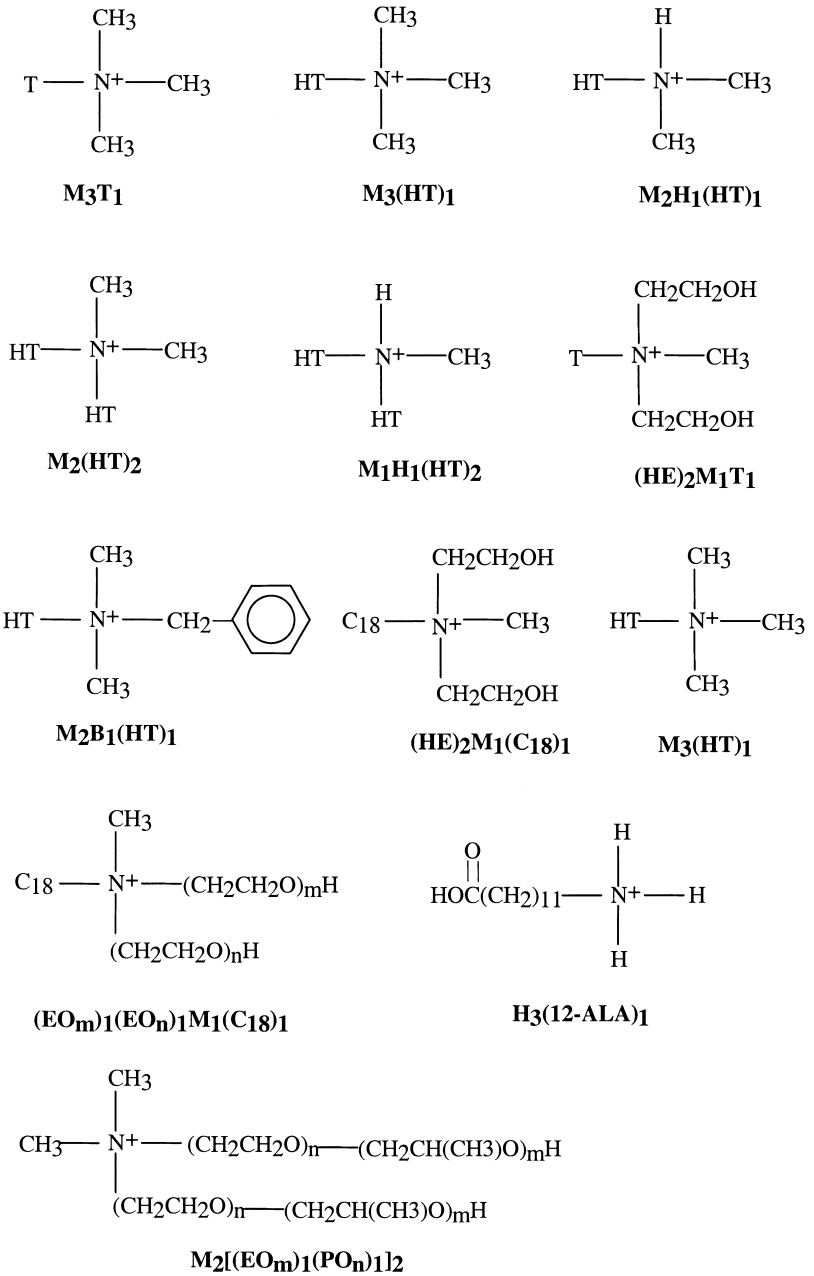

Fig. 1. (a) Molecular structure and nomenclature of amine salts used to organically modify sodium montmorillonite by ion exchange. The substituents on the nitrogen are designated, sing M = methyl, T = tallow, (HT) = hydrogenated tallow, (HE) = 2-hydroxy-ethyl, B = benzyl, (C_{18}) = octadecyl hydrocarbon, (EO) = ethylene oxide, (PO) = propylene oxide, (12-ALA) = 12-amino laulic acid, and H = hydrogen.

with digital data acquisition. An extensiometer with a 2.54 cm gauge length was used to determine modulus and yield strength. Elongation at break was measured at a crosshead speed of 5.1 cm/min. Standard or sharp notched Izod impact tests were performed using a 6.8 J hammer and 3.5 m/s impact velocity at room temperature using a TMI Izod tester. Standard notches were made according to ASTM D256 while sharp notches were made by tapping a new razor blade into the center of the machined standard notch. Typically, data from six specimens were averaged to determine mechanical properties with error limits of the order of 4% for modulus, 1–2% for yield strength, and 20% for elongation at break.

2.5. Wide angle X-ray diffraction

WAXD was conducted using a Sintag XDS 2000 diffractomer in the reflection mode using an incident X-ray wavelength of 1.542 Å at a scan rate of 1.0 deg/min. X-ray analysis was performed on Izod bars except for the organoclay itself, which was in powder form.

Table 2
Organoclays used in this study

Organoclay	SCP Designation	Chemical structure	Specifications
$(HE)_2M_1T_1$	Cloisite® 30B[a]	Bis(2-hydroxy-ethyl)methyl tallow ammonium montmorillonite	90 MER, organic content = 31.5 wt%, d_{001} = 17.9 Å
$(HE)_2M_1(C_{18})_1$	Experimental	Bis(2-hydroxy-ethyl)methyl octadecyl ammonium montmorillonite	95 MER, organic content = 29.7 wt%, d_{001} = 18.2 Å
M_3T_1	Experimental	Trimethyl tallow ammonium montmorillonite	95 MER, organic content = 29.1 wt%, d_{001} = 17.8 Å
$M_3(HT)_1$	Experimental	Trimethyl hydrogenated-tallow ammonium montmorillonite	95 MER, organic content = 29.6 wt%, d_{001} = 18.0 Å
$M_2H_1(HT)_1$	Experimental	Dimethyl hydrogenated-tallow ammonium montmorillonite	95 MER, organic content = 28.9 wt%, d_{001} = 17.1 Å
$M_1H_1(HT)_2$	Experimental	Methyl bis(hydrogenated-tallow) ammonium montmorillonite	95 MER, organic content = 38.4 wt%, d_{001} = 24.3 Å
$M_2(HT)_2$	Cloisite® 20A	Dimethyl bis(hydrogenated-tallow) ammonium montmorillonite	95 MER, organic content = 31.5 wt%, d_{001} = 24.2 Å
M_2 B_1 $(HT)_1$	Experimental	Dimethyl benzyl hydrogenated-tallow ammonium montmorillonite	95 MER, organic content = 31.1 wt%, d_{001} = 18.6 Å
$H_3(12\text{-}ALA)_1$	Experimental	12-Aminolauric acid ammonium montmorillonite	95 MER, organic content = 23.2 wt%, d_{001} = 13.5 Å
$(EO_m)_1(EO_n)_1M_1(C_{18})_1$	Experimental	Bis(polyoxyethylene)methyl octadecyl ammonium montmorillonite	95 MER, organic content = 46.6 wt%, d_{001} = 18.1, 35.2 Å, $m+n=15$
$M_2[(EO)_5(PO)_5]_2$	Experimental	Dimethyl bis(ethylene oxide-co-propylene oxide) ammonium montmorillonite	95 MER, organic content = 61.7 wt%, d_{001} = 18.1 Å
$M_2[(EO)_2(PO)_8]_2$	Experimental	Dimethyl bis(ethylene oxide-co-propylene oxide) ammonium montmorillonite	60 MER, organic content = 37.7 wt%

[a] Cloisite® is a registered trademark of Southern Clay Products.

2.6. Electron microscopy

Samples for TEM analysis were taken from the core portion of an Izod bar perpendicular to the flow direction. Ultrathin sections approximately 50 nm in thickness were cut with a diamond knife at room temperature using a Reichert-Jung Ultracut E microtome. Sections were collected on 300 mesh gold grids and subsequently dried with filter paper. The sections were examined by TEM at an accelerating voltage of 80 kV using a JOEL 2010F TEM equipped with a Field Emission Gun.

3. Effect of polycarbonate molecular weight on nanocomposite mechanical properties

Fig. 2 shows the effect of montmorillonite (MMT) loading on the modulus of the nanocomposite, E, relative to the modulus of the polycarbonate matrix, E_m. For comparison, similar data for nylon 6 nanocomposites based on a high molecular weight (HMW) nylon 6 matrix are also shown. Note that all data are reported in terms of the weight percent of montmorillonite in the composite rather than the amount of organoclay, since the silicate is the reinforcing component. The organoclay used to form nanocomposites with both matrices was Cloisite® 30B, $(HE)_2M_1T_1$. The compounding was performed at 240 °C for nylon 6 and 260 °C for polycarbonate nanocomposites. The torque required to turn the screw of the extruder for polycarbonate was similar to that for nylon 6. Rheological measurements indicate that the shear stress exerted on the clay particles should be similar, e.g. 200 kPa at 100 s^{-1} [15,17]. The nylon 6 nanocomposites have higher relative moduli than the polycarbonate nanocomposites. Typically, the modulus of these polycarbonate nanocomposites containing 3 wt% MMT loading is improved by about 35%; while in the case of nylon 6, modulus is increased by about 50%. Evidently there is a higher degree of exfoliation of the organoclay in nylon 6 than in polycarbonate. More direct evidence of the morphological state of the clay in the polycarbonate nanocomposites by X-ray diffraction and TEM will be described later.

Fig. 3 shows the effect of the molecular weight of the polycarbonate matrix on the modulus (a), relative modulus (b), yield strength (c), elongation at break (d), and Izod impact strength (e) of nanocomposites formed from the organoclay based on the $(HE)_2M_1T_1$ surfactant; also see Table 3. As seen in Table 1, the weight average molecular weight of polycarbonate matrix is 23,000 g/mol for medium molecular weight polycarbonate (MMW-PC) and 32,000 g/mol for high molecular weight polycarbonate (HMW-PC). It is interesting to note in Fig. 3(a) that the pure MMW-PC has a higher modulus than HMW-PC; Kayano observed the same trend for these materials [16]. This counter-intuitive result may stem from the more narrow distribution of molecular weight of the MMW-PC than HMW-PC, i.e. 2.3

Table 3
Mechanical properties of polycarbonate nanocomposites based on $(HE)_2M_1T_1$

	MMW-PC					HMW-PC				
MMT (%)	0	1.6	2.6	3.3	4.7	0	1.5	2.5	3.4	4.4
Modulus (GPa)	2.33	2.62	2.83	2.98	3.31	2.15	2.561	2.81	3.0	3.27
Yield (MPa)	60.5	64.5	66.8	68.3	N/A	58.4	63.2	65.7	67.3	70.5
Elongation (%)[a]	127.5	68.5	32.6	8.0	4.5	144.2	91.0	79.2	50.0	13.0
IZOD Impact (J/m)	949.1	72.5	62.2	44.9	35.0	825.0	60.9	47.2	29.7	27.1

[a] Cross head speed = 5.1 cm/min.

for MMW-PC and 2.8 for HMW-PC. The moduli of the nanocomposites formed from the MMW and HMW PC overlap each other but the slopes of the modulus curves are different. To eliminate this difference between the two PC matrices, Fig. 3 (b) shows the relative moduli versus MMT loading. Clearly, HMW-PC leads to nanocomposites with somewhat greater modulus enhancement than MMW-PC. Similar observations were reported previously for nanocomposites based on nylon 6 [15]. It was suggested that the higher modulus of the nanocomposites results from the higher melt viscosity of the molten matrix polymer as its molecular weight increased. At a fixed RPM of the extruder screw, i.e. fixed shear rates, the higher melt viscosity leads to higher stresses during melt processing which in turn leads to more efficient exfoliation of clay platelets [15]. Note that the melt viscosities of HMW-PC and MMW-PC at $\dot{\gamma} = 100\ 1/s$, are 2,000 and 1,100 Pa S, respectively, measured at the compounding temperature of 260 °C [17]. Based on the data and model described earlier [15], it is reasonable that the HMW-PC is more effective for exfoliation of the organoclay and in turn shows greater reinforcement. The yield strength of the nanocomposites formed from HMW-PC and MMW-PC, see Fig. 3(c), show completely analogous trends as seen for the modulus both in terms of absolute and relative values. Based on the elongation at break data in Fig. 3(d), the nanocomposites formed from HMW-PC retain a higher level of ductility in slow tensile tests than those formed from MMW-PC which is also consistent with what was found in nylon 6 nanocomposites [15]. The nanocomposites formed from MMW-PC showed brittle failure at 3.3% MMT while those formed from HMW-PC showed ductile failure at 3.3% MMT and then brittle failure at 4.4% MMT. As seen by the solid lines of Fig. 3(e), addition of only small amounts of organoclay causes a significant drop in the standard notch impact strength from the very high value of 1000 J/m for neat polycarbonate to about 40 J/m at 4.5% MMT loading. The nanocomposites based on HMW-PC have higher impact strength than those based on MMW-PC which might be expected based on Fig. 3(d). The response of the impact strength, measured on samples with a standard Izod notch, to the addition of organoclay is quite different for polycarbonate than found earlier for nylon 6 [15]. This stems partly from the fact that neat nylon 6, while ductile in simple tensile tests, is brittle in the standard Izod test while neat polycarbonate remains very ductile in this test. Addition of clay to polycarbonate rapidly diminishes this ductility leading to brittle fractures in the Izod test for nanocomposites due either to the restraints caused by exfoliated platelets or defect-like character that stems from

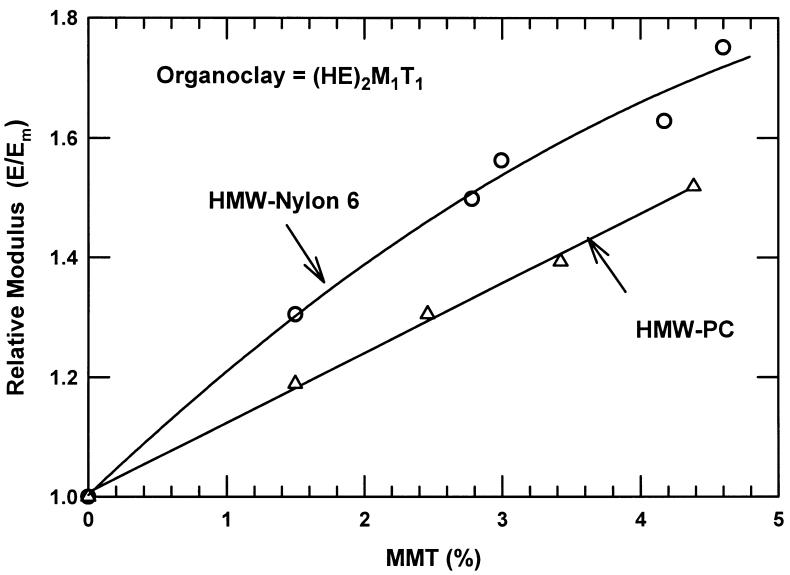

Fig. 2. Relative modulus as a function of montomorillonite content of nanocomposites formed from HMW nylon 6 (○) and HMW polycarbonate (△) made by melt processing using a twin screw extruder. The organoclay used here was prepared from the $(HE)_2M_1T_1$ surfactant.

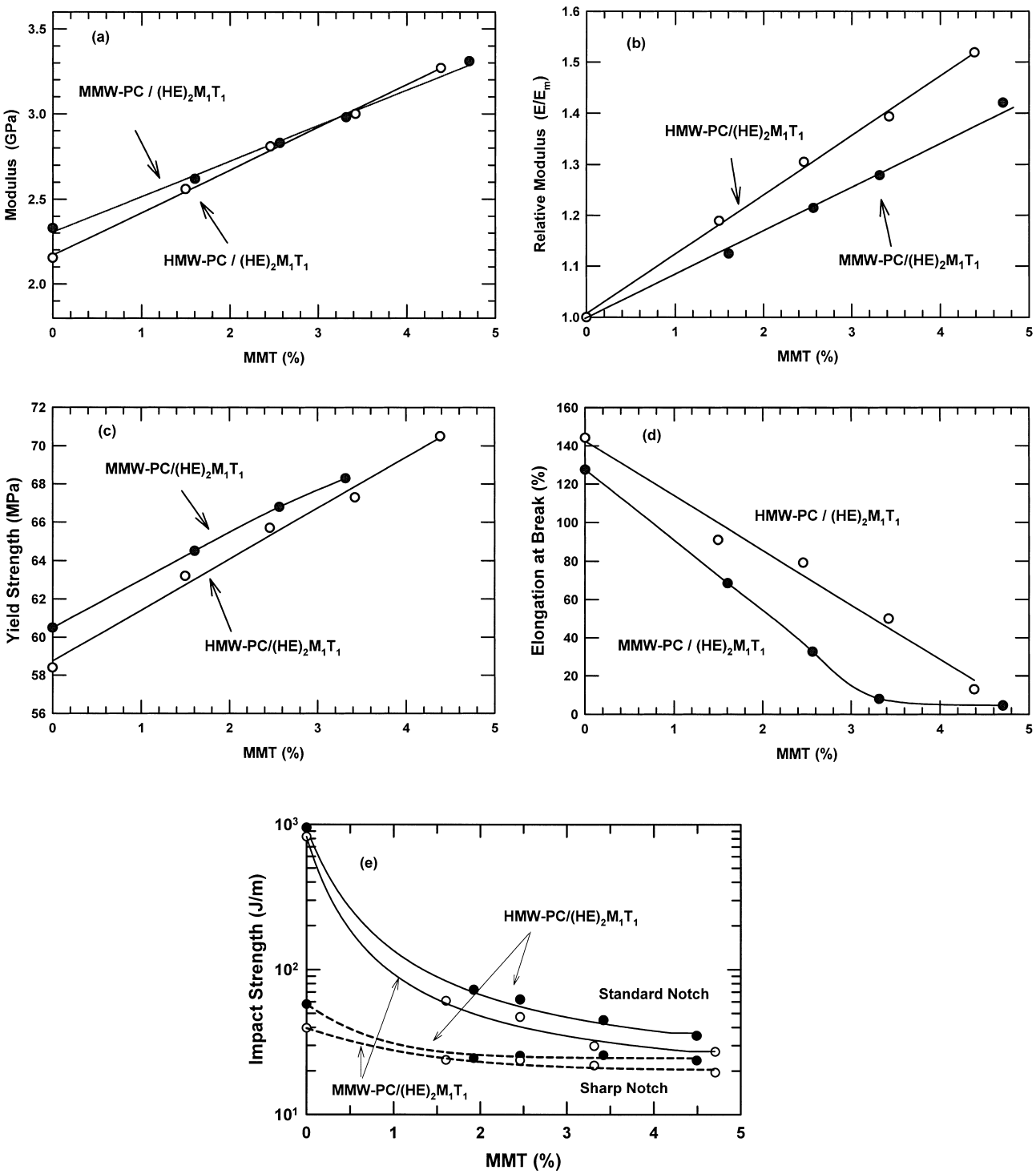

Fig. 3. (a) Tensile modulus, (b) relative modulus, (c) yield strength, (d) elongation at break, (e) standard and sharp notch impact strength for MMW-PC (●) and HMW-PC (○) based nanocomposites.

larger clay particles or both. Polycarbonate shows brittle behavior in the Izod test when the notch is sharper than the standard one or the specimen is thicker due to a transition from plane stress to plane strain conditions [20,21]. Therefore, a more reasonable way to examine the response of adding clay to polycarbonate is to use a sharp notch so that comparisons are made at comparable conditions of plane strain. The dotted lines in Fig. 3(e) show the sharp notch impact strength. The sharp notch causes neat HMW-PC and MMW-PC to fracture in a brittle manner with impact strengths of ~60 and ~40 J/m, respectively. Adding clay causes a slight decrease in the impact strength up to about 1.6% MMT loading and then remains constant at higher contents of MMT. The nanocomposites based on

HMW-PC show higher impact strength than those based on MMW-PC for specimens with either the sharp or standard notch.

Based on the higher stiffness and ductility for the nanocomposites formed from HMW-PC, the remainder of this study concerning the effect of organoclay structure on morphology and physical properties was limited to nanocomposites formed from the HMW-PC matrix.

4. Effect of organoclay structure on nanocomposite morphology and mechanical properties

4.1. Overview

The structure of the organic amine compound used to form the organoclay is expected to have some effect on the morphology and properties of the nanocomposites based on polycarbonate. The morphology of these materials as determined by direct TEM observations is summarized in Section 4.3. To explore the mechanical properties, two target MMT loadings were chosen, 2.4 and 4.5 wt% (or 1.03 and 1.96 vol%) in the present experiments that use HMW-PC as the matrix. Fig. 4 shows the moduli for the nanocomposites prepared from the various modified organoclays; as might be expected, sodium montmorillonite causes that least improvement in stiffness while the organoclay formed from $(EO_m)_1(EO_n)_1M_1(C_{18})_1$ gives the highest enhancement. The other organoclays fall between these two limits.

For direct comparisons, it is necessary to have tight control of MMT concentration in the nanocomposites. In most cases, the MMT loadings determined by ash content were close to the target value, but in a few cases the actual values were somewhat different as shown in Table 4. To correct for this, we assumed a linear relationship between each mechanical property and MMT content in the range of 2–5% to interpolate or extrapolate to the target loadings; the resulting values are summarized in Table 5. To obtain an overview of the results and the trade-offs involved, Fig. 5 shows the yield strength (a), elongation at break (b), impact strength (c) versus modulus, while Fig. 5(d) shows elongation versus impact strength; all plots are based on the data from Table 4. Broadly speaking, the yield strength of the HMW-PC nanocomposites increases with the modulus, as shown in Fig. 5(a), indicating that incorporation of clay into polycarbonate improves both stiffness and strength in an analogous manner. Similar results were found in nylon 6 nanocomposites prepared with some of the same organoclays examined in the current study [15]. On the other hand, elongation at break shows a trade-off relationship with stiffness, see Fig. 5(b), as observed in the previous paper for nylon 6 nanocomposites. Since both are related to material ductility, impact strength shows a similar pattern as the elongation at break, i.e. generally there is a decrease in both measures of ductility as modulus increases.

4.2. Thermal stability of organoclay

It would be interesting to interpret the properties described above in terms of the morphology of the composites as determined by WAXS and TEM. However, before attempting to do this, it is important to recognize that these materials were processed at 260 °C which is a very high temperature in view of the well-known thermal stability issues of quaternary amine compounds [22,23].

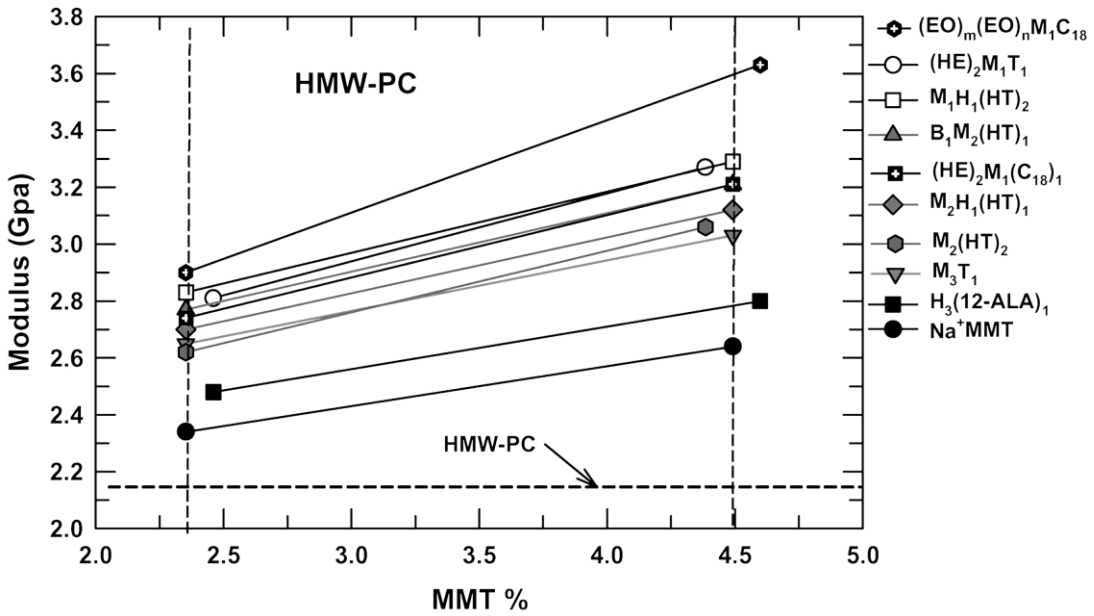

Fig. 4. Modulus as a function of montmorillonite content for nanocomposites formed from HMW-PC with various organoclays. The dashed vertical lines represent experimental target MMT loading levels in weight%.

Table 4
Mechanical properties of polycarbonate nanocomposites

Clay	MMT (%)	Modulus (Gpa)	Yield Strength (Mpa)	%Elong@ Break 0.2″/min	%Elong@ Break 0.2″/min
Pure E2000	0	2.15	58.4	–	144.0
$(HE)_2M_1T_1$	2.5	2.81	66.2	–	81.5
	4.4	3.27	70.5	–	13.0
$(HE)_2M_1(C_{18})_1$	2.4	2.74	66.3	–	104.5
	4.5	3.21	70.2	–	12.9
$M_3(HT)_1$	1.9	2.65	62.8	–	63.8
	4.4	3.08	[a]	–	4.7
$M_1H_1(HT)_2$	2.4	2.83	64.2	118.4	113.9
	4.5	3.29	65.9	60.7	27.9
$M_2B_1(HT)_1$	2.4	2.77	63.7	82.6	96.3
	4.5	3.21	66.7	6.6	10.7
M_3T_1	2.4	2.65	63.0	86.7	88.6
	4.5	3.03	65.1	21.6	14.5
$M_2H_1(HT)_1$	2.4	2.70	62.5	106.5	114.2
	4.5	3.12	65.3	13.1	11.7
$M_2(HT)_2$	2.4	2.62	61.4	81.9	86.0
	4.4	3.06	63.8	9.8	9.9
$(EO_m)_1(EO_n)_1M_1(C_{18})_1$	2.4	2.90	64.4	–	74.9
	4.6	3.63	[a]	–	2.64
$M_2[(EO)_2(PO)_8]_2$	2.2	2.40	60.2	–	100
$M_2[(EO)_5(PO)_5]_2$	2.8	2.82	66.4	–	36.2
$H_3(12\text{-}ALA)_1$	2.5	2.48	60.9	–	100.0
	4.6	2.80	62.0	–	80.9
Na^+MMT	2.4	2.34	59.7	–	105
	4.5	2.64	61.7	–	70.0

[a] Specimen failed before yield.

To examine the thermal stability of organoclays at high temperatures, the following experiments were motivated largely by a mysterious peak in the X-ray scans at a d-spacing of ~ 14 Å seen in all the PC-based nanocomposites prepared in this study. The organoclay $(HT)_2M_2T_1$ was heat-treated at 250 °C by pressing at 6.9 kPa in a compression molding press for various lengths of time; the resulting changes in the X-ray scan for this organoclay

Table 5
Mechanical properties of nanocomposites formed from HMW-PC and various organoclays

HMW-PC/Oganoclay nanocomposite		Modulus (GPa)	Yield strength (MPa)	Elongation at break (%)	Impact strength (J/m)
$(HE)_2M_1T_1$	2.4 wt% MMT	2.79	66.0	85.4	83.9
	4.5 wt% MMT	3.31	70.7	9.0	34.1
$(HE)_2M_1(C_{18})_1$	2.4 wt% MMT	2.74	66.3	104.5	63.4
	4.5 wt% MMT	3.21	70.2	12.9	38.1
M_3T_1	2.4 wt% MMT	2.65	63.0	88.6	86.7
	4.5 wt% MMT	3.03	65.1	14.5	21.6
$M_3(HT)_1$	2.4 wt% MMT	2.74	64.2	54.0	50.7
	4.5 wt% MMT	3.10	N/A	4.9	26.3
$M_2H_1(HT)_1$	2.4 wt% MMT	2.70	62.5	114.2	75.7
	4.5 wt% MMT	3.12	65.3	11.7	40.0
$M_1H_1(HT)_2$	2.4 wt% MMT	2.83	64.2	113.9	117.5
	4.5 wt% MMT	3.29	65.9	27.9	69.4
$M_2(HT)_2$	2.4 wt% MMT	2.62	61.4	86.0	114.2
	4.5 wt% MMT	3.08	63.9	5.68	46.7
$M_2\ B_1\ (HT)_1$	2.4 wt% MMT	2.77	63.7	96.3	61.9
	4.5 wt% MMT	3.21	66.7	10.7	37.3
$H_3(12\text{-}ALA)_1$	2.4 wt% MMT	2.46	60.8	100.1	–
	4.5 wt% MMT	2.78	61.9	81.9	–
$(EO_m)_1(EO_m)_1M_1(C_{18})_1$	2.4 wt% MMT	2.90	64.4	74.9	58.2
	4.5 wt% MMT	3.60	N/A	6.1	19.5
Na^+MMT	2.4 wt% MMT	2.34	59.7	105	110.0
	4.5 wt% MMT	2.64	61.7	70.0	70.0

Data have been interpolated or extrapolated to the targeted MMT loading levels when necessary.

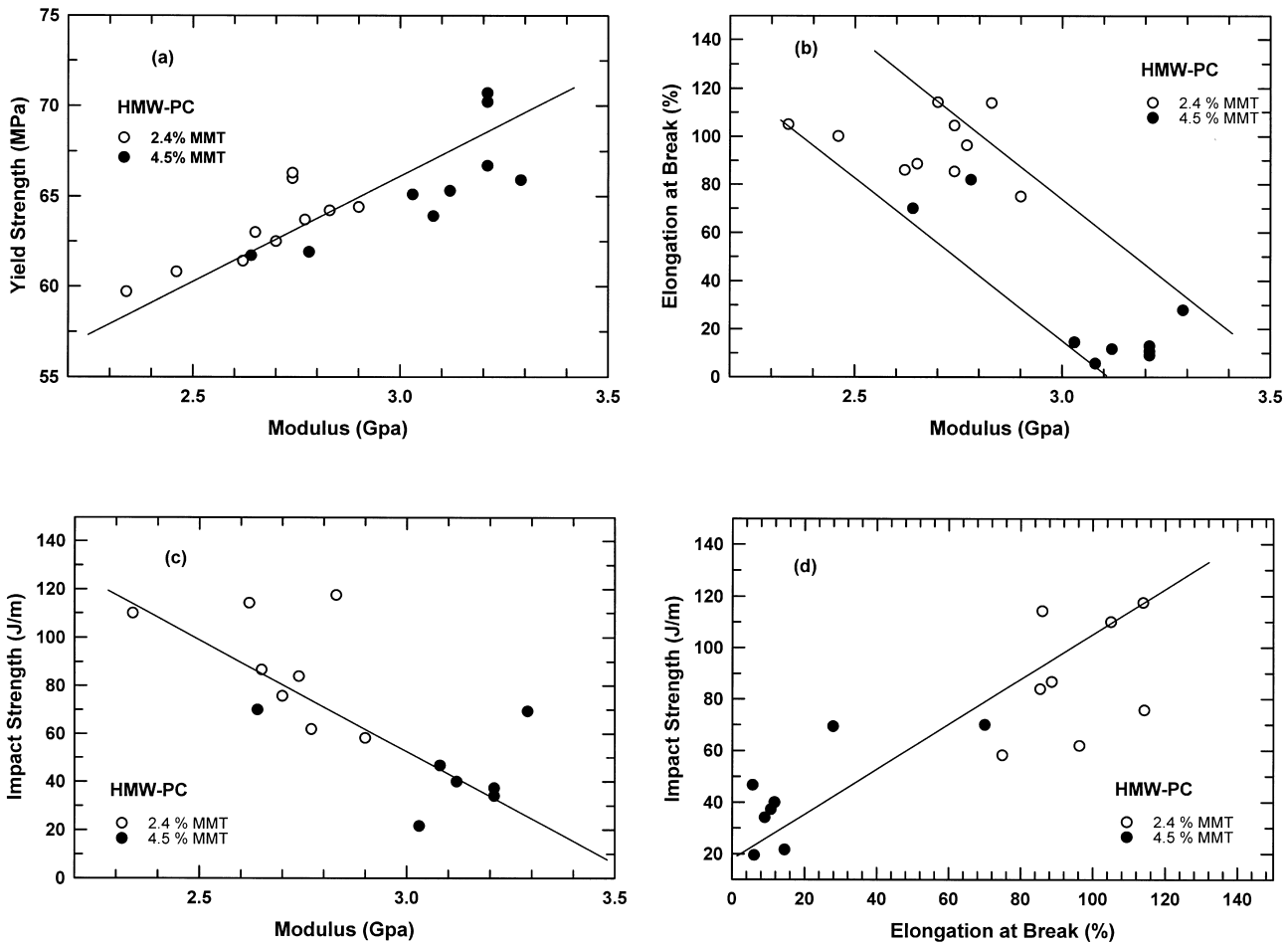

Fig. 5. Relationships between (a) yield strength and modulus, (b) elongation at break and modulus, (c) impact strength and modulus, and (d) impact strength and elongation at break for HMW-PC based nanocomposites.

are shown in Fig. 6. The pristine organoclay shows two peaks; d_{001} at 25.6 Å and d_{002} at 12.4 Å. Heating for 1 min did not cause a noticeable change in the platelet spacing. The organoclay turned increasingly darker shades of brown with annealing time in the hot press indicative of thermal degradation processes. After 5 min of heating, the d_{001} platelet spacing increased from 25.6 Å to about 31 Å and the peak broadened indicating a less regular structure. However, the peak now appearing at about 13 Å probably does not correspond to a shifted d_{002} peak seen in the pristine organoclay since it is larger in magnitude; it may relate to degradation of the quaternary ammonium compound. On further heating, this peak occurs at about 14 Å and grows in intensity relative to the d_{001} peak as seen Fig. 6. Based on these facts, we believe the 14 Å peak is the result of some clay galleries containing degraded organic material. If the organic material were completely lost, then the basal d-spacing of montmorillonite, 9.6 Å, should appear, but it does not. It is suggested that a carbonaceous material forms in the galleries propping the platelets apart as the quaternary ammonium decomposes at high temperature. VanderHart found, using solid-state NMR, both quaternary ammonium on the clay surface and residue from the decomposed quaternary ammonium in the matrix of nylon 6 nanocomposites [22]. The results shown here strongly suggest that the peak at 14 Å represents a partially collapsed structure from quaternary ammonium degradation.

4.3. TEM observations of morphology

Fig. 7 shows TEM photomicrographs of nanocomposites formed from the organoclays H_3(12-ALA)$_1$ (a), M_3T_1 (b, c), and $(EO_m)_1(EO_n)_1M_1(C_{18})_1$ (d) which represent the lowest, intermediate and highest moduli, respectively, observed in this study, see Fig. 4. The composite formed from H_3(12-ALA)$_1$ contains many large aggregates of micron size like the one shown in the center of Fig. 7(a); however, the majority of the particles are smaller than this. The particles in this material range in length from 0.2 to 5 μm. In order to give some sense of the average particle size and aspect ratio, the dimensions of approximately 40 particles were measured with the number average values shown in Table 6. Similar large particles also are found in composites formed from Na^+MMT, and the modulus enhancement for sodium montmorillonite is about the same as for H_3(12-ALA)$_1$ as seen in Fig. 4. The carboxyl groups on the amino

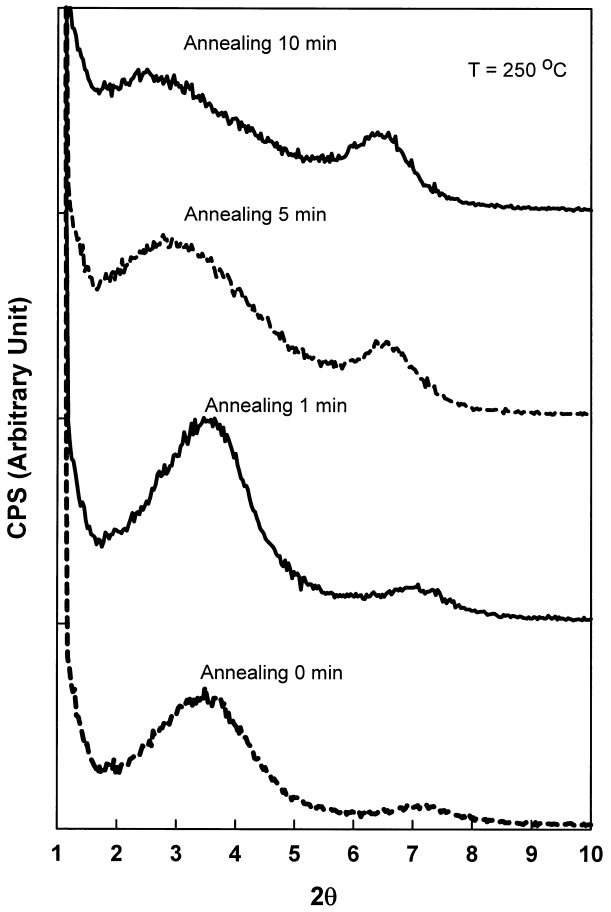

Fig. 6. WAXS results for the pristine organoclay, $M_2(HT)_2$, thermally treated for various periods at 250 °C in a compression molding press.

lauric acid surfactant could be thought to react with the polycarbonate to from polymer grafts to the aluminosilicate platelets which, in principle, should be beneficial for exfoliation; however, clearly no such benefit is observed. It should be also pointed out that the d-spacing of this pristine organoclay, 13.5 Å, is even lower than the 14 Å d-spacing of the collapsed structure discussed in Section 4.2.

Fig. 7(b) shows the morphology of the nanocomposites formed from the M_3T_1 surfactant. Most of the particles in this material are much smaller than observed for H_3(12-ALA)$_1$-based materials having an average length and thickness of 312 nm and 25 nm, respectively. These particles are of the type referred to as 'tactoids', and X-ray data shown later reveals some intercalation of polymer into the galleries. However, large aggregates like the one marked by the arrow in the photomicrograph can be seen throughout the section even though these are not the main population of particles. There is no evidence of single aluminosilicate platelets in these materials. The large aggregates seem to be somewhat loosely packed as seen in Fig. 7(c). This structure might correspond to the peak at $2\theta = 6°$ in the X-ray scan to be discussed later. In addition to their dimension and shape, it is in interesting to see that the particles are less aligned in the flow direction than those formed in a nylon 6 matrix [24].

Fig. 7(d) shows the structure of PC nanocomposites formed using the $(EO_m)_1(EO_n)_1M_1(C_{18})_1$ surfactant. This material has the smallest clay particles of any of the composites reported here; the average particle dimensions are 217 nm (l) and 8 nm (t). The TEM photomicrograph reveals that most of the dispersed particles are thin tactoids containing several aluminosilicate layers while there seem to be a few single platelets shown by the arrows in Fig. 7(d). These *partially exfoliated* platelets are well aligned to the flow direction. Clearly, most tactoids contain multiple platelets; however, a detailed quantitative analysis is difficult due to the lack of perfect alignment to the electron beam that causes shadows at the edge and makes it almost impossible to count layers. The aspect ratio of dispersed particles was based on the ratio of average length to average thickness as summarized in Table 6. Theoretical composite models predict that aspect ratio plays an important role in controlling reinforcement [25,26]. The relative values of modulus enhancement seen in Fig. 4 can be related to the progression of aspect ratios seen in Table 5 as the organoclay is changed from H_3(12-ALA)$_1$ to M_3T_1 to $(EO_m)_1(EO_n)_1M_1(C_{18})_1$.

4.4. Effect of number of long alkyl groups

In this and following subsections, we attempt to show how each structural feature of the organic modifier affects morphology and properties by altering the groups attached to the nitrogen one at the time in a systematic manner as we described previously for a nylon 6 matrix [15]; however, because the degree of dispersion is much lower for PC nanocomposites, the trends are more difficult to interpret. Fig. 8 shows WAXS scans (a), modulus (b), and elongation at break (c) data for the HMW-PC nanocomposites based on organoclays having one long alkyl (one tail) versus two alkyl groups (two tails), i.e. $M_3(HT)_1$ versus $M_2(HT)_2$ and $M_2H_1(HT)_1$ versus $M_1H_1(HT)_2$, respectively. The WAXS

Table 6
Average dimensions of particles in nanocomposites formed from selected organoclays as determined by TEM

Organoclay	Average length (nm)	Average thickness (nm)	Aspect ratio[a]
H_3(12-ALA)$_1$	910	370	2.5
M_3T_1	312	25	12.5
$(EO_m)_1(EO_n)_1M_1(C_{18})_1$	217	8	26.6

[a] Aspect ratio = (average length)/(average thickness).

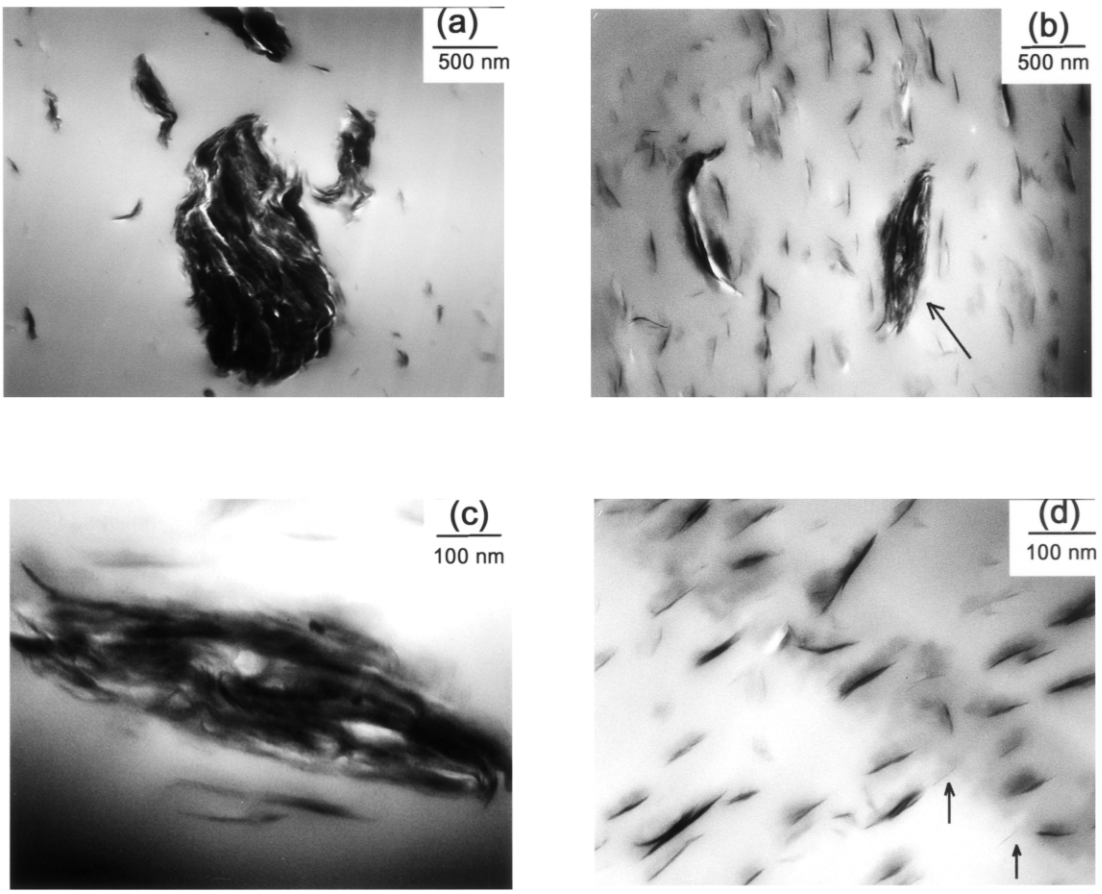

Fig. 7. TEM photomicrographs of nanocomposites formed from the organoclays (a) $H_3(12\text{-}ALA)_1$, (b) and (c) M_3T_1, and (d) $(EO_m)_1(EO_n)_1M_1(C_{18})_1$.

scans in Fig. 8(a) show that nanocomposites formed from these organoclays contain some intercalated structures. Each blend shows two basal reflections; the peak at around $2\theta \cong 3°$ corresponds to an interlayer spacing of 30 Å and may result from intercalation of polycarbonate molecules into the gallery while the peak at $2\theta = 6°$ may represent the collapse of some galleries caused by decomposition of the organic component as discussed above or a multiple reflection. On blending with polycarbonate, the organoclay having one alkyl tail shows a larger increase in basal spacing than those containing two alkyl tails. The pristine organoclay with one tail $M_3(HT)_1$ has a d_{001} spacing of 18.0 Å which increases by 12.4 Å on blending with PC; on the other hand, the organoclay with two tails $M_2(HT)_2$ has a d_{001} spacing of 24.2 Å in the pristine state that increases by only 5.7 Å on blending with PC. Another comparison can be made with tertiary amine compounds; the interlayer spacing for $M_2H_1(HT)_1$ increases by 14.1 Å while for $M_1H_1(HT)_2$ the increase is 4.5 Å.

The modulus data for the nanocomposites shown in Fig. 8(b) indicates that $M_1H_1(HT)_2$ leads to the greatest and $M_2(HT)_2$ the least modulus enhancement while $M_3(HT)_1$ and $M_2H_1(HT)_1$ lead to intermediate enhancements that are essentially equivalent. One tail leads to better enhancement in stiffness in the nanocomposites formed from the quaternary ammonium series while two tails give more modulus enhancement in nanocomposites formed from the tertiary ammonium series. The elongation at break data in Fig. 8(c) shows better retention of ductility by the two tertiary amines, $M_1H_1(HT)_2$ and $M_2H_1(HT)_1$, than the two quaternary amines, $M_2(HT)_2$ and $M_3(HT)_1$. Within the same amine class, the two tail structures give higher ductility for both the tertiary and quaternary amines. Of these organoclays, $M_1H_1(HT)_2$ gives both the highest modulus and the highest elongation at break.

4.5. Hydroxy-ethyl versus methyl

Fig. 9 compares the morphologies and tensile properties for nanocomposites based on organoclays having 2-hydroxy-ethyl versus methyl substituents, i.e. $(HE)_2M_1T_1$ versus M_3T_1. As seen in the top half of Fig. 9(a), the organoclay, M_3T_1, has a peak at $2\theta = 5°$ which corresponds to a d-spacing of 17.8 Å. On blending with HMW-PC, the platelet spacing increases to 30.9 Å as judged by the peak at $2\theta = 2.8°$ and a new peak at $2\theta = 6°$ emerges which is the 14 Å spacing described earlier and attributed to degradation. As seen in the lower half of Fig. 9(a), the organoclay, $(HE)_2M_1T_1$, has an X-ray peak at $2\theta \sim 5°$ corresponding to a gallery spacing of 17.9 Å. On blending with HMW-PC,

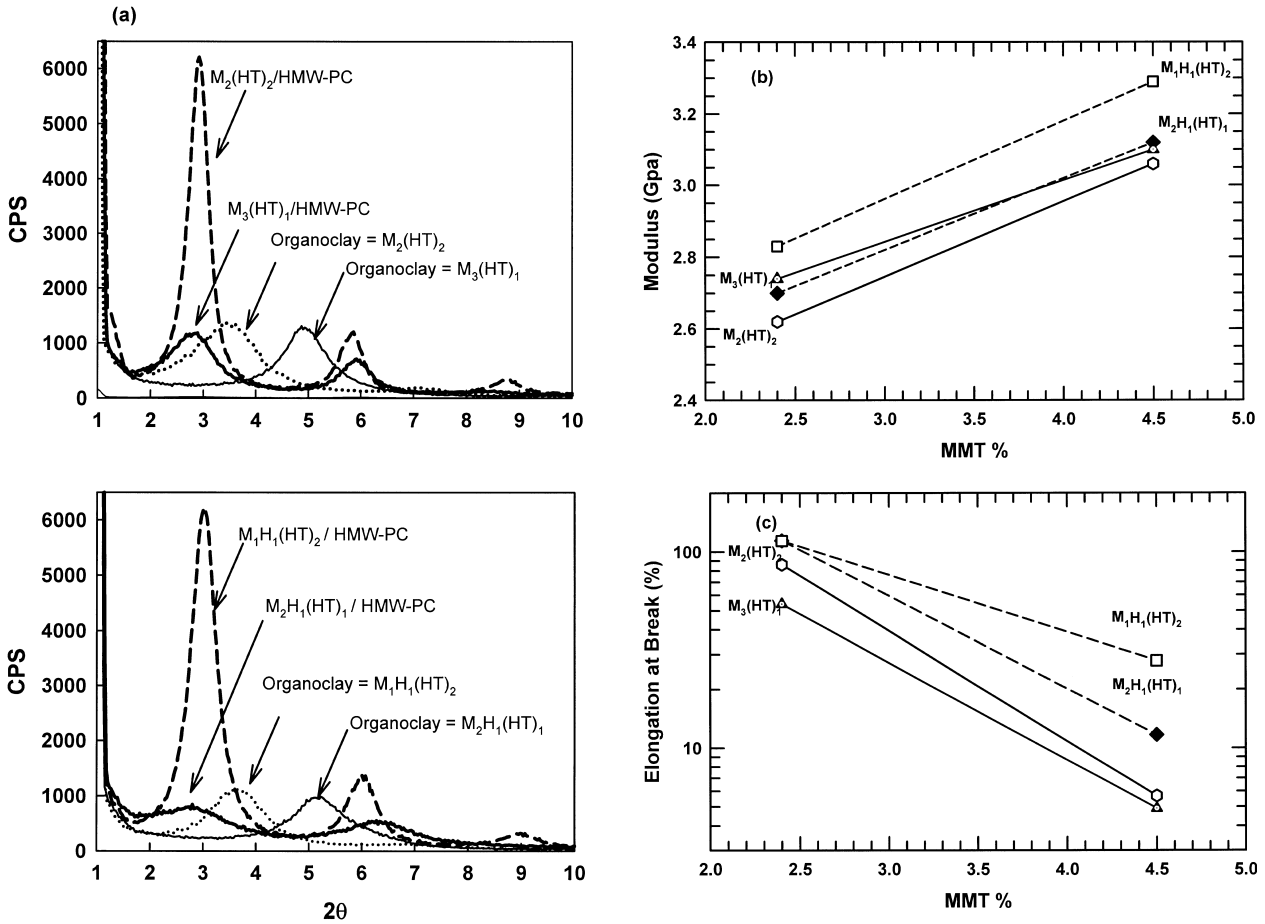

Fig. 8. (a) WAXS scans, (b) modulus, and (c) elongation at break data for the HMW-PC nanocomposites based on organoclays having one long alkyl (one tail) versus two alkyl groups (two tails): $M_3(HT)_1$ versus $M_2(HT)_2$ and $M_2H_1(HT)_1$ versus $M_1H_1(HT)_2$.

this peak seems to disappear altogether while the 14 Å peak emerges as seen in all other PC-nanocomposites. The absence of the low angle peak for the $(HE)_2M_1T_1$ nanocomposite would seem to suggest that the organoclay is exfoliated; however, direct observation by TEM reveals tactoids with some large aggregates. It is interesting to note that the TEM images show the particles to be less well-aligned than for other nanocomposites, which may explain the absence of a peak in the X-ray scan.

Fig. 9(b) shows that the nanocomposites based on the structure having hydroxy-ethyl groups has a significantly higher modulus than the corresponding modification where methyl groups are present. On the other hand, nanocomposites based on M_3T_1 have slightly higher elongations at break than those based on $(HE)_2M_1T_1$.

While the cause and effect relationships are less clear, it is instructive to compare the properties of nanocomposites based on $M_3(HT)_1$ versus those based on $(HE)_2M_1T_1$. Fig. 10 compares relative modulus (a), yield strength (b), elongation at break (c), and impact strength (d). The nanocomposites based on $(HE)_2M_1T_1$ clay shows slightly higher modulus, better yield strength, higher elongation at break, and impact strength. Of course, this comparison also involves native tallow tail (T) versus a hydrogenated version (HT) in addition to the methyl versus hydroxy-ethyl.

4.6. Effect of ethylene and propylene oxide tails

This section describes results obtained using a novel organoclay based on a quaternary ammonium modifier having one C_{18} alkyl tail plus two short chains of poly(ethylene oxide) and a methyl group; this structure is designated as $(EO_m)_1(EO_n)_1M_1(C_{18})_1$ where the average values of m plus n are 15; this surfactant, thus, has three tails. The nanocomposites based on this surfactant will be compared with those based on the analogous surfactant $(HE)_2M_1(C_{18})_1$ without poly(ethylene oxide) units and with $(HE)_2M_1T_1$. Organoclays based on poly(propylene oxide), $M_2[(EO_5)(PO_5)]$ and $M_2[(EO_2)\ (PO_8)]$, will also be compared. Fig. 11 compares nanocomposites from $(EO_m)_1$-$(EO_n)_1M_1(C_{18})_1$ with those formed from $(HE)_2M_1(C_{18})_1$. As seen in the top half of Fig. 11(a), the organoclay based on $(HE)_2M_1(C_{18})_1$ gives a basal spacing of 18.2 Å. Nanocomposites formed from it have a weak, poorly defined peak at about $2\theta = 3°$ or 30 Å plus the usual 14 Å believed to be associated with degradation. This is reminiscent of the

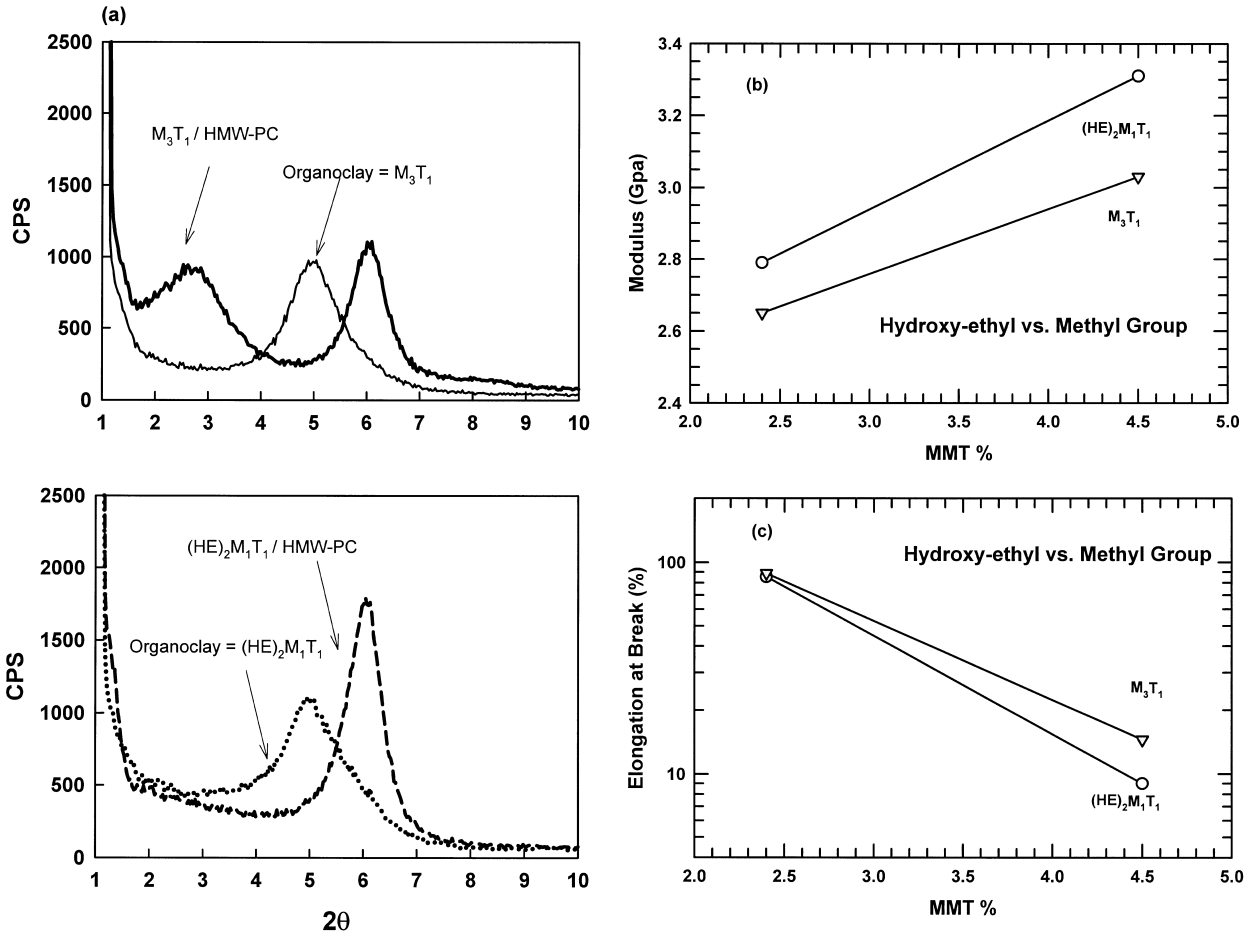

Fig. 9. (a) WAXS scans, (b) modulus, and (c) elongation at break data for the HMW-PC nanocomposites based on organoclays having hydroxy-ethyl, $(HE)_2M_1T_1$, versus methyl groups, M_3T_1.

results for $(HE)_2M_1T_1$ as seen in Fig. 9(a). On the other hand, the organoclay based on $(EO_m)_1(EO_n)_1M_1(C_{18})_1$ has peaks at about $2\theta = 2.1$ and 5° or d-spacings of 35.2 and 18.1 Å which moves to 32.2 Å on blending with PC. According to an empirical relation of organoclay d-spacing versus the surfactant molecular weight reported earlier [15], the pristine organoclay based on $(EO_m)_1(EO_n)_1M_1(C_{18})_1$ would be expected to have a d-spacing of 35.1 Å. The fact that this organoclay has two separate d-spacings suggests that the surfactant may not have a simple, single structure; in fact, subsequent discussions with the supplier of this surfactant revealed that it contains some free poly(ethylene oxide). The literature reveals the higher molecular weight poly(ethylene oxide) spontaneously intercalates into the galleries of montmorillonite to give a basal spacing of 18 Å [4–6,27,28]. Thus, we believe that this impurity causes the d-spacing of 18 Å. TEM images shows intercalated tactoids and a proportion of partially exfoliated platelets for the nanocomposites based on $(EO_m)_1(EO_n)_1M_1(C_{18})_1$, These nanocomposites have the best platelet dispersion among materials prepared in this study, and the stiffness levels shown Fig. 11(b) reflect this. The nanocomposites based on $(EO_m)_1(EO_n)_1M_1(C_{18})_1$ shows the highest modulus of any composites in this study. Note that the $(EO_m)_1(EO_n)_1$-$M_1(C_{18})_1$ nanocomposite containing 2.2% MMT has a modulus about 35% higher than that of neat HMW-PC; this is almost comparable to the degree of reinforcement found for nylon 6 nanocomposites. The higher modulus enhancement for polyethylene oxide-based clay may be due to the fact that polyethylene oxide and polycarbonate are miscible while the poor modulus enhancement for poly(ethylene oxide-co-propylene oxide) based clays may reflect lack of miscibility between poly(propylene oxide) and polycarbonate [29–31]. As might be expected, the elongation at break values for the nanocomposites based on $(EO_m)_1(EO_n)_1$-$M_1(C_{18})_1$ are relatively low.

4.7. Quaternary versus tertiary ammonium treatments

Fig. 8 also shows the effects of forming organoclays from quaternary versus tertiary ammonium compounds by ion exchange with sodium montmorillonite. Two comparisons can be made: $M_3(HT)_1$ versus $M_2H_1(HT)_1$and $M_2(HT)_2$ versus $M_1H_1(HT)_2$. The X-ray scans show intercalated morphologies for both pairs with only small differences in structure as seen in Fig. 8(a). Each nanocomposite has a

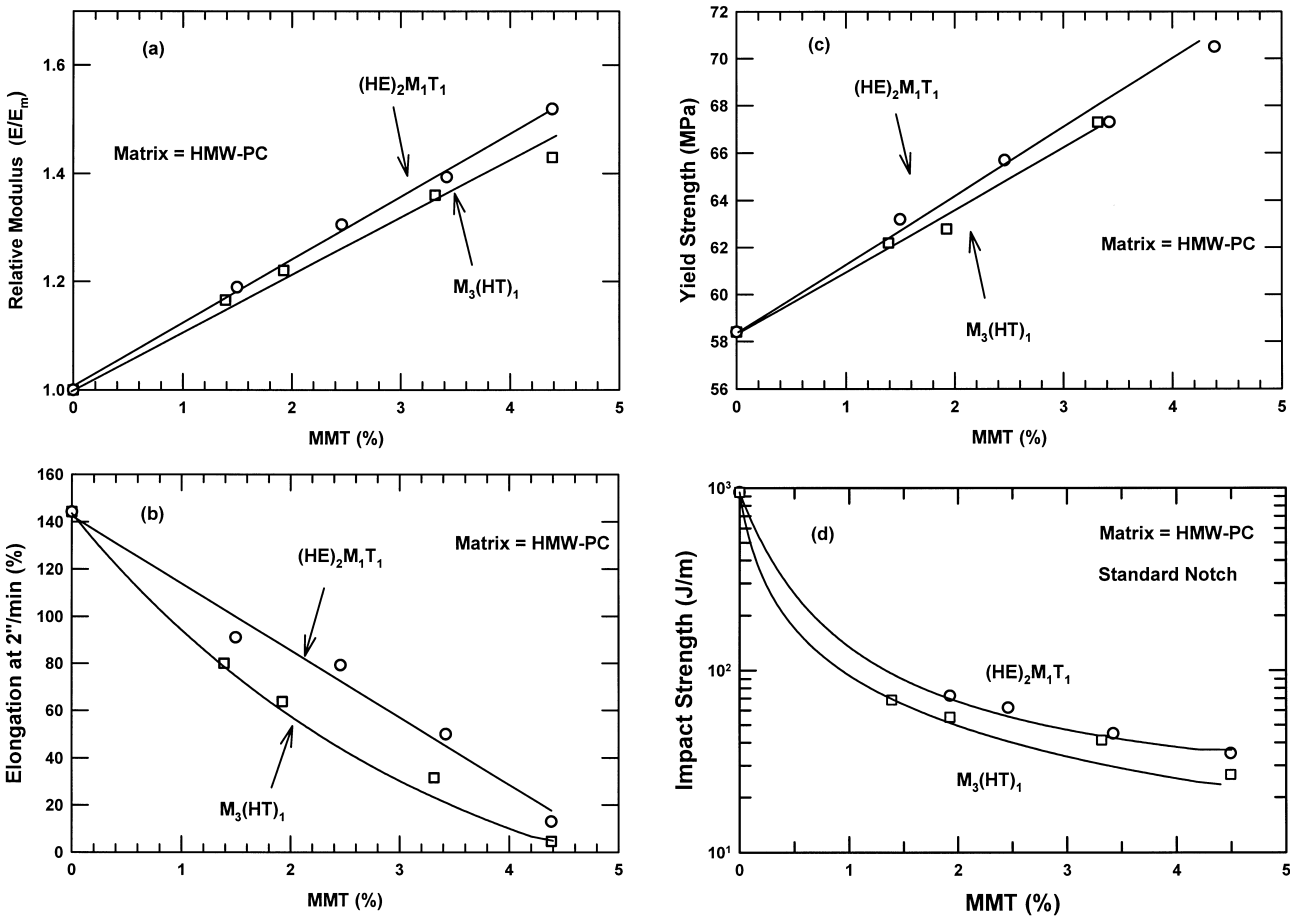

Fig. 10. (a) Relative modulus, (b) elongation at break, (c) yield strength, (d) standard notch impact strength for the HMW-PC nanocomposites based on organoclays having $(HE)_2M_1T_1$ and $M_3(HT)_1$ surfactants.

peak at $2\theta \sim 3°$ due to polymer intercalated galleries plus the 14 Å peak. The peak at $2\theta = 9°$ in Fig. 8(a) and (b) is only seen in nanocomposites formed from organoclays having two tails, i.e. $M_2(HT)_2$ and $M_1H_1(HT)_2$. This may be secondary diffraction from the strong peak at $2\theta \sim 3°$ or $\sim 6°$. Fig. 8(b) shows that the nanocomposites based on the tertiary amine $M_1H_1(HT)_2$ have higher stiffness than the those based on the quaternary ammonium $M_2(HT)_2$. However, there is very little difference between $M_3(HT)_1$ versus $M_2H_1(HT)_1$. It is interesting to see in Fig. 8(b) and (c) that $M_2H_1(HT)_1$ results in both higher stiffness and elongation at break.

4.8. Saturated tallow effects

The long tallow tails on the amine surfactants are made from natural oil that contains some unsaturation, i.e. double bonds. This unsaturation may lead to undesired chemical reactions particularly at the high temperature used in melt processing. To examine these effects on the physical properties of HMW-PC nanocomposites, surfactants with hydrogenated tallow units, designated as (HT), were used. These products contain a small residual unsaturation; however, the ammonium compound $(HE)_2M_1(C_{18})_1$ should be essentially free of unsaturation. Saturated versus unsaturated alkyl groups in the organoclay can be analyzed by comparing $M_3(HT)_1$ versus M_3T_1 and $(HE)_2M_1T_1$ versus $(HE)_2M_1(C_{18})_1$. X-ray diffraction patterns and TEM photomicrographs show no significant difference in the intercalated structures between the saturated and unsaturated structures. Nanocomposites based on $M_3(HT)_1$ have slightly higher modulus than those based on M_3T_1 as may be seen in Table 5. Nanocomposites formed from $M_3(HT)_1$ show higher elongation at break than those formed from M_3T_1 as seen in Table 6 In the $(HE)_2M_1T_1$ versus $(HE)_2M_1(C_{18})_1$ case, there is more than just hydrogenation to consider; tallow has a distribution of the number of carbons with the average being about 18 carbons while C_{18} has no such distribution. In nylon 6, nanocomposites formed from $M_3(HT)_1$ show a slight advantage in modulus compared to the unstaturated clay based on M_3T_1. However, hydrogenation can be very beneficial for controlling degradation of the surfactant and subsequently the polymer matrix, which will be discussed in the subsequent paper.

4.9. Effect of benzyl groups

The substituent size (or volume) on a surfactant can

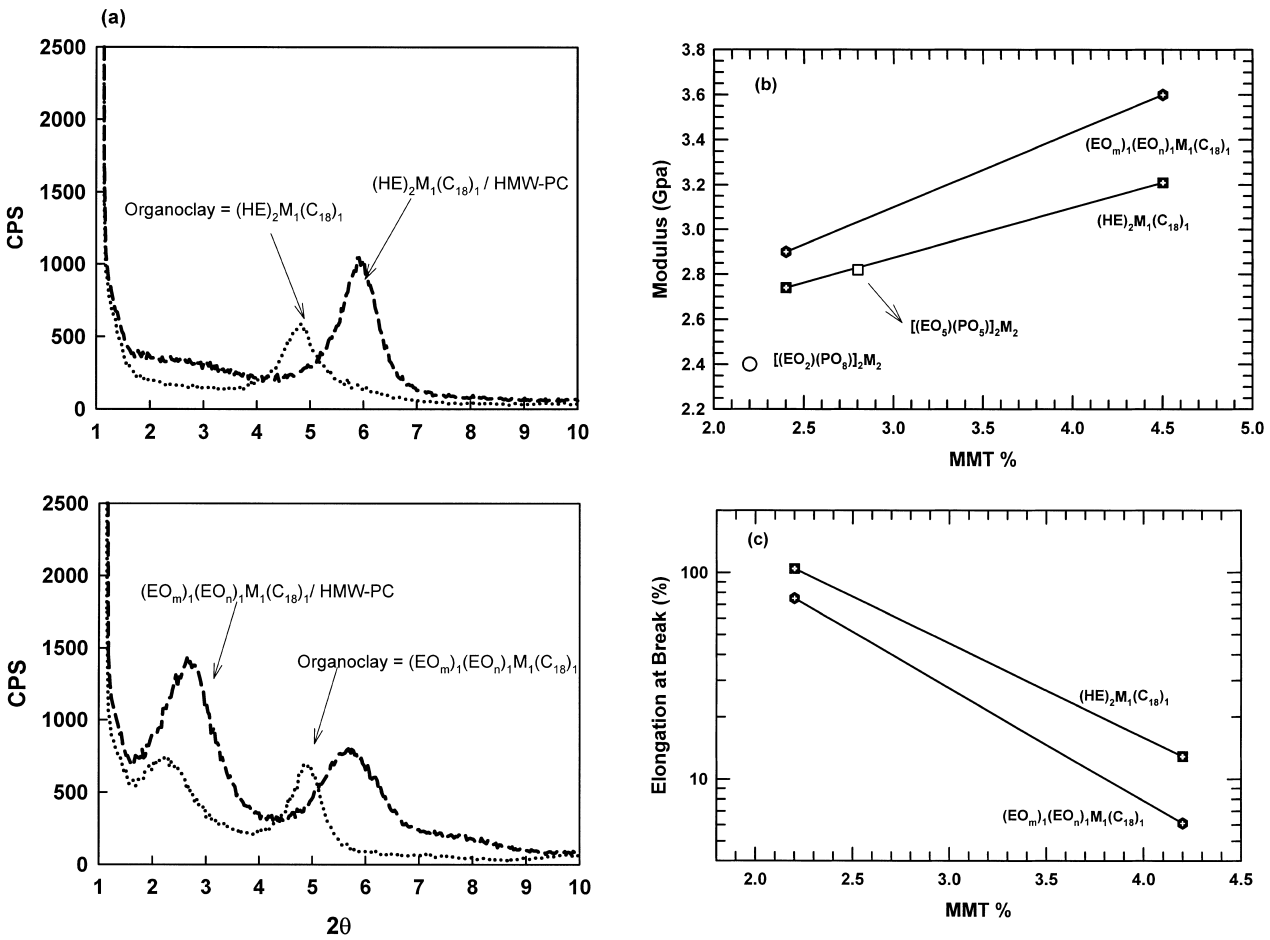

Fig. 11. (a) WAXS scans, (b) modulus, and (c) elongation at break data for the HMW-PC nanocomposites formed from organoclays having hydroxy-ethyl, $(HE)_2M_1(C_{18})_1$, and poly(ethylene oxide), $(EO_m)_1(EO_n)_1M_1(C_{18})_1$ units.

affect the dispersion of clay particles in the polymer matrix. Here we consider the general structure $(M)_2X_1(HT)_1$ where X is either a hydrogen, methyl, or benzyl group. X-ray data reveals that the pristine organoclay based on a benzyl group shows slightly higher d-spacing, 18.6 Å, than the ones based on methyl and hydrogen, 18.0 and 17.1 Å, respectively. However, no significant difference was found in the intercalated structures for the nanocomposites based on these surfactants. There is little difference in the modulus of PC nanocomposites when X = hydrogen or methyl while the benzyl group gives a slightly higher modulus. It is interesting to see that the material with a benzyl group also has a higher elongation at break than do the methyl or hydrogen substituted organoclays, see Tables 4 and 5.

5. Effects of physical structure of clay and nanocomposites on mechanical properties

In addition to the organoclay chemical structure, physical structure may play a role in exfoliation or intercalation in a polymer matrix. Intuitively, one might expect that the further the aluminosilicate platelets are pushed apart by ion exchange with the organic modifier (i.e., the larger the organoclay d-spacing) the easier it will be to obtain intercalation by the polymer or exfoliation; see data in Table 7. However, a recent study of nylon 6 nanocomposites showed that tensile modulus or yield strength did not increase with the d-spacing of the organoclay; if anything, the opposite trend was found [15]. This study indicated that better exfoliation stems from a good affinity of the polymer for the organoclay rather than larger platelet separation in the pristine organoclay. Some of the same organoclays used in the nylon 6 investigation [15] were used to prepare polycarbonate nanocomposites for this study.

Fig. 12(a) shows the tensile modulus of polycarbonate nanocomposites (at a fixed content of MMT of 4.5%) versus the d-spacing the pristine organoclay. Most of organoclay gallery heights are distributed near 18 Å except for H_3(12-ALA)$_1$ at 12 Å, $M_1H_1(HT)_2$ and $M_2(HT)_2$ at 24 Å, and $(EO_m)_1(EO_n)_1M_1(C_{18})_1$ at 35.2 Å (ignoring the 18.1 Å peak attributed to an impurity). Organoclays with $d_{001} \sim 18$ Å have a single alkyl tail with 18 carbon atoms (average values for T and HT); within this series, the modulus increases as the size of the other substituents increase, i.e. HE > B > M. Overall, one might conclude that modulus

Table 7
X-ray d-spacings for organoclays and their polycarbonate nanocomposites containing 4.5% MMT

Clays	Clay d_0	Primary peak	Second peak
Na^+MMT	9.6	11.2	–
H_3(12-ALA)$_1$	13.5	14.0	–
$M_2(HT)_2$	24.2	29.9	15.1
$(HE)_2M_1(C_{18})_1$	18.2	–	14.9
$M_1H_1(HT)_2$	24.3	28.8	14.7
$M_3(HT)_1$	18.0	30.4	14.9
$M_2H_1(HT)_1$	17.1	31.2	14.1
M_3T_1	17.8	30.1	14.6
$M_2B_1(HT)_1$	18.6	28.6	14.5
$(HE)_2M_1T_1$	17.9	(35.3)	14.6
$(EO_m)_1(EO_n)_1M_1(C_{18})_1$	18.1/35.2	32.2	15.3

enhancement increase as the organoclay d_{001} spacing increases; however, this apparent trend is heavily influenced by the result for $(EO_m)_1(EO_n)_1M_1(C_{18})_1$ which is believed to reflect the miscibility of the short poly(ethylene oxide) tails with polycarbonate. This physical interaction is probably more important than is the d-spacing per se.

Fig. 12(b) shows a plot of the nanocomposite tensile modulus versus the d-spacing observed in the nanocomposite. There seems to be some trend of nanocomposite stiffness with this parameter. A definitive cause and effect relationship is difficult to establish; however, we can speculate as follows. The d-spacing in the nanocomposite is indicative of the amount of polycarbonate that is intercalated into the tactoids of organoclay clearly visible in TEM photomicrographs and detected by X-rays. This parameter, to some extent, reflects the affinity of the organoclay for polycarbonate and this no doubt correlates with the number platelets that are exfoliated or, at least, the smaller the number of platelets in each tactoid. The degree of reinforcement increases as both the number of particles and their aspect ratio increase as the clay becomes better dispersed in the polycarbonate matrix.

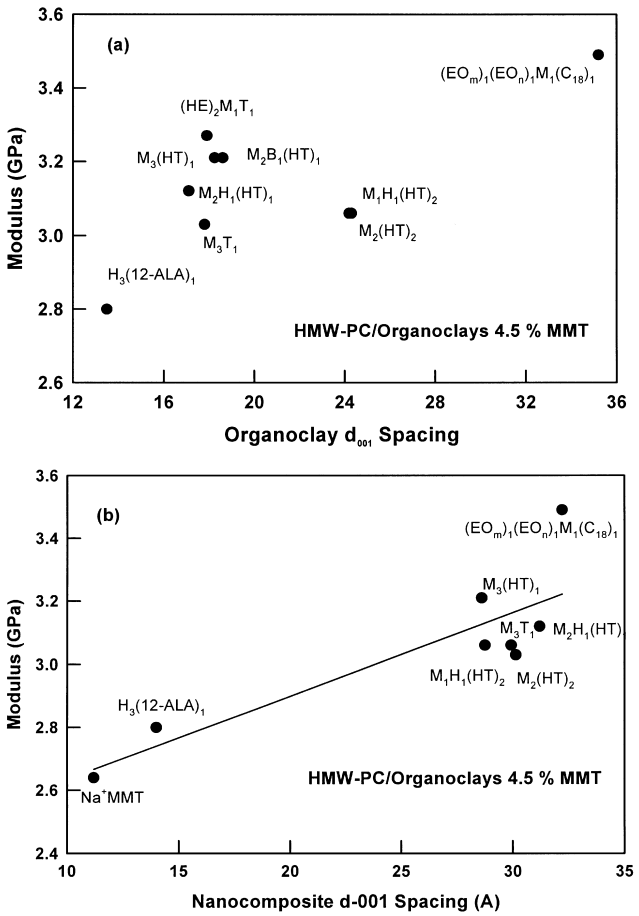

Fig. 12. Plots of nanocomposite modulus versus organoclay d-spacing (a) before and (b) after mixing with polycarbonates.

6. Conclusions

Organoclay nanocomposites based on HMW-PC and MMW-PC were prepared by melt processing to explore the effect of matrix molecular weight. Tensile test shows HMW-PC gives better stiffness and ductility in the nanocomposite than MMW-PC. The higher melt viscosity and consequently higher shear stress is believed to be the major contributor to higher modulus in the HMW-PC nanocomposites.

Structure-property relations for nanocomposites formed from a series of organoclays and HMW-PC are also presented here. The chemical structure of the alkyl ammonium surfactants was systematically varied to determine how specific groups might affect polycarbonate nanocomposite properties. As seen by X-ray, most of the organoclays give two distinct structures, i.e. $2\theta = 2-3°$ (29–44 Å) and $2\theta \sim 6°$ (~15 Å); the former peak is assigned to tactoids containing intercalated polymer while the latter is believed to be particles containing collapsed platelet caused by thermal degradation of the organic surfactant. TEM photomicrographs reveal mostly the tactoids having several platelets and sometimes large aggregates.

The surfactant having polyoxyethylene and octadecyl alkyl tails shows the most significant improvement in modulus and leads to partially exfoliated platelets in TEM microphotographs. This exfoliation of platelets is attributed to the miscibility of the poly(ethylene oxide) tail with PC. This result points to organoclays with tails miscible with the matrix polymer as a pathway for polycarbonate nanocomposites with high levels of platelet exfoliation.

Acknowledgements

This work was supported by the Air Force Office of Scientific Research, the Texas Advanced Technology Program, and Mitsubishi Engineering Plastics Corp. The authors would like to thank Randy Chapman and Benjamin

Knesek of Southern Clay Products for their help with WAXS and TEM analysis.

References

[1] Alexandre M, Dubois P. Mater Sci Engng 2000;28:1–63.
[2] Furuichi N, Kurokawa Y, Fujita K, Oyo A, Yasuda H, Kiso M. J Mater Sci 1996;31:4307–10.
[3] Kurokawa Y, Yasuda H, Kashiwagi M, Oyo A. J Mater Sci Lett 1997; 16:1670–2.
[4] Adanda P, Ruiz-Hitzky E. Chem Mater 1992;4:1395–403.
[5] Vaia RA, Vasudevan S, Krawiec W, Scanlon LG, Giannelis EP. Adv Mater 1995;7:154–6.
[6] Vaia RA, Sauer BB, Tse OK, Giannelis EP. J Polym Sci, Polym Phys 1997;35:59–67.
[7] Yoon JT, Jo WH, Lee MS, Ko MB. Polymer 2001;42:329–36.
[8] Huang J, Zhu Z, Qian X, Sun Y. Polymer 2001;42:873–7.
[9] Zanetti M, Camino G, Thomann R, Mulhaupt R. Polymer 2001;42: 4501–7.
[10] Alexandre M, Beyer G, Henrist C, Cloots R, Rulmont A, Jerome R, Dubois P. Macromol Rapid Commun 2001;22:643–6.
[11] LeGrand DG, Bendler JT. Handbook of polycarbonate science and technology. New York: Marcel Dekker; 2000.
[12] Huang X, Lewis S, Brittain WJ, Vaia RA. Macromolecules 2000;33: 2000–4.
[13] Severe G, Hsieh AJ, Koene BE. 58th ANTEC 2000;2:1523–6.
[14] Fornes TD, Yoon PJ, Keskkula H, Paul DR. Polymer 2001;42: 2121–2.
[15] Fornes TD, Yoon PJ, Hunter DL, Keskkula H, Paul DR. Polymer 2002;43:5915–33.
[16] Kayano Y, Keskkula H, Paul DR. Polymer 1996;37:4505–18.
[17] Yoon PJ, Hunter DL, Paul DR. Polymer 2003:10.1016/S0032-3861(03)00523-8.
[18] Long TS, Sokol RJ. Polym Engng Sci 1974;14:817–22.
[19] GE Plastics Technical Brochure 'Lexan Processing Guide'
[20] Cheng TW, Keskkula H, Paul DR. J Appl Polym Sci 1992;45:531.
[21] Lombardo BS, Keskkula H, Paul DR. J Appl Polym Sci 1994;54: 1697–720.
[22] VanderHart DL, Asano A, Gilman JW. Macromolecules 2001;34: 3819–22.
[23] Xie W, Gao Z, Pan W, Hunter DL, Singh A, Vaia RA. Chem Mater 2001;13:2979–90.
[24] Yoon PJ, Fornes TD, Paul DR. Polymer 2002;43:6727–41.
[25] Ashton JF, Halpin JC, Petit PH. Primer composite materials analysis. USA: Technomic; 1969.
[26] Chow TS. J Polym Sci, Polym Phys 1978;16:959–65.
[27] Lemmon JP, Wu J, Oriakhi C, Lerner MM. Electrochimica Acta 1995; 40:13–14.
[28] Shen Z, Simon GP, Cheng Y. Polymer 2002;42:4251–60.
[29] Brus J, Dybal J, Schmidt P, Kratochvil J, Baldrian J. Macromolecules 2000;33:6448–59.
[30] Lin J, Cheng I, Wang R, Lee R. Macromolecules 2001;34:8832–4.
[31] Saito S. Polymer-surfactant interactions. In: Schick MJ, editor. Nonionic surfactants. New York: Marcel Dekker; 1987. Chapter 15.